

Article

Bridgeless PFC Converter without Electrolytic Capacitor Based on Power Decoupling

Ning-Zhi Jin ^{1,*}, Zhi-Qiang Wu ¹, Long Zhang ¹, Yu Feng ¹ and Xiao-Gang Wu ^{1,2,*}

¹ Engineering Research Center of Automotive Electronics Drive Control and System Integration, Ministry of Education, Harbin University of Science and Technology, Harbin 150080, China

² State Key Laboratory of Automotive Safety and Energy, Tsinghua University, Beijing 100084, China

* Correspondence: sharon0716@126.com (N.-Z.J.); xgwu@hrbust.edu.cn (X.-G.W.)

Abstract: Due to fewer conduction devices in operating condition, the bridgeless power factor correction (PFC) converter is more efficient than the traditional PFC circuit. However, to achieve a low output voltage ripple on the DC side, a large electrolytic capacitor must be connected in parallel to the output end. To reduce the value of capacitance, this paper proposes a dual-boost bridgeless PFC converter with a bidirectional buck/boost power decoupling converter in the latter stage. The bidirectional converter absorbs double-line-frequency ripple, lowering the power pulsation at the output end while realizing power decoupling. The one-cycle control is adopted in bridgeless PFC converter, so that the input current can follow the input voltage to achieve power factor correction and decrease harmonic pollution. The power decoupling circuit is designed with a voltage outer loop using PI control and a current inner loop using model predictive current control, which alleviates the output voltage fluctuation caused by the reduction of the capacitance value of the filter capacitor, for the purpose of realizing non-electrolytic capacitor. Finally, the topology and control strategy involved in this paper are simulated and experimented to verify the validity and superiority of the theory.

Keywords: bridgeless PFC; power decoupling; non-electrolytic capacitor; one cycle control; model predictive current control



Citation: Jin, N.-Z.; Wu, Z.-Q.; Zhang, L.; Feng, Y.; Wu, X.-G. Bridgeless PFC Converter without Electrolytic Capacitor Based on Power Decoupling. *Electronics* **2023**, *12*, 321. <https://doi.org/10.3390/electronics12020321>

Academic Editor: Sara Deilami

Received: 23 November 2022

Revised: 27 December 2022

Accepted: 5 January 2023

Published: 8 January 2023



Copyright: © 2023 by the authors. Licensee MDPI, Basel, Switzerland. This article is an open access article distributed under the terms and conditions of the Creative Commons Attribution (CC BY) license (<https://creativecommons.org/licenses/by/4.0/>).

1. Introduction

With rapid development in power electronic technology, the use of power electronic equipment has increased daily, and the problem of harmonic pollution to the power grid has become more grievous [1,2]. The suppression of harmonics has attracted attention from domestic and foreign experts. Power factor correction (PFC) technology has gained a lot of attention and research from many domestic and foreign researchers due to its potential to suppress current harmonics, such that the input current and voltage are in the same phase and are in sine wave [3–7]. In the traditional PFC converter, there are three on/off switches present at any given moment. The on-state loss increases significantly when the switching frequency of the system is large. In the bridgeless PFC converter [8,9], the two diodes of the rectifier bridge are replaced by the power switching devices, and only two switching devices are left turned on at all times. The on-state loss of the system is reduced, the efficiency is significantly improved, and the power factor correction effect is comparable to that of the traditional PFC [10–12]. The PFC converter traditionally adopts average current control, peak current control, hysteresis current control, etc., [13,14]. All of these controls use analog multipliers, which complicates the control circuit, whereas the one cycle control (OCC) does not require a multiplier, which simplifies control and improves system efficiency and power density [15,16]. With the continuous development of microprocessor technology and increasing computing speed, some novel controls, such as fuzzy control and model predictive control, have been more widely studied in the field of power electronics [17–19].

However, similar to traditional PFC converters, bridgeless PFC converters also need to be connected to large electrolytic capacitors in parallel at the output to reduce output voltage fluctuations. The large volume of electrolytic capacitors not only increases the size of the converter but also reduces the reliability and service life of the system. With the increasing demand for converter performance, the development of technology without an electrolytic capacitor is particularly important.

A new type of unipolar topology using coupled inductors, which could be used to achieve no electrolytic capacitors, was introduced in reference [20]. However, the circuit structure and control method becomes complicated due to the addition of coupled inductors. A composite buck/boost PFC converter was proposed to suppress the output double-line-frequency ripple in reference [21]. Compared with the traditional two-stage cascade, this topology reduces a group of switches and driving circuits, resulting in the power factor reaching 0.99. However, there is a disadvantage of a relatively low energy transfer efficiency in this circuit. A series LC network was used for replacing the electrolytic capacitors, filtering out some specific ripple currents through resonance, and absorbing excess pulsating power in the circuit in reference [22]. However, a large inductance is usually required since the ripple current frequency is generally low. Gu et al. [23] adopts the method of increasing the voltage ripple of the filter capacitor and injecting the third harmonic current into the input current to reduce the capacitance value of the capacitor. However, the loss increases as the harmonic current is injected into the system. The two methods are combined according to the actual situation. A power decoupling circuit in parallel on the DC side, to absorb double-line-frequency pulsating power of the AC input to achieve no electrolytic capacitors, was proposed in references [24–30]. The system is popularly used in electrolytic capacitor-less technology, which is more efficient than the cascaded two-stage topology.

In this paper, a bidirectional buck/boost power decoupling circuit is added based on the dual-boost bridgeless PFC converter with one cycle control. A double-loop control of voltage outer loop using PI control and current inner loop using model predictive current control (MPCC) is proposed for the power decoupling converter. It is controlled to absorb double-line-frequency ripple power, which reduces the output power ripple, realizes power decoupling, and achieves the purpose of removing electrolytic capacitors. Finally, the validity and superiority of the theory are verified by simulations and experiments.

2. Working Principle and Control Strategy of Dual Boost Bridgeless PFC Converter

A bridgeless PFC converter incorporating a power decoupling circuit is shown in Figure 1. The topology consists of two parts, a dual-boost bridgeless PFC converter for AC/DC conversion, and a bidirectional buck/boost power decoupling circuit is added to the output end of the bridgeless PFC, which absorbs the low-frequency ripple power, reduces the output voltage ripple of the DC bus, reduces the capacitance value of the filter capacitor, ensures no electrolytic capacitor, and increases the service life of the entire machine. The working principles of the dual-boost bridgeless PFC converter and the bidirectional buck/boost power decoupling circuit are described below.

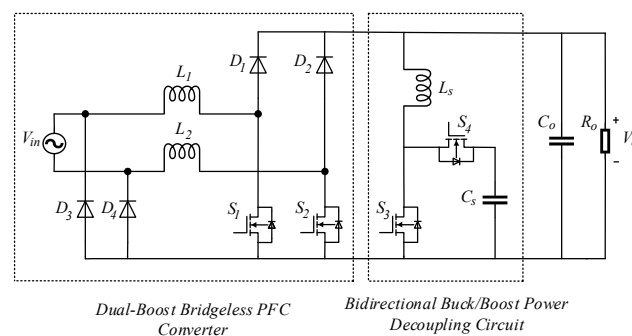


Figure 1. Dual-boost bridgeless PFC converter based on power decoupling.

2.1. Working Principle

The dual-boost bridgeless PFC can be considered as a boost PFC converter in the positive or negative half cycle of the power frequency AC input. Therefore, the same driving signal is used for controlling the switches S1 and S2. The power factor correction is realized by controlling the duty ratio of S1 and S2, and the converter is controlled to output a constant DC voltage. In one switching cycle, the dual-boost bridgeless PFC converter can be divided into four operating states.

State I: As shown in Figure 2a, $V_{in} > 0$, switch S1 is turned on, and S2 is turned off. At this point, the input current flows back to the power supply through L_1 , S1, D4, and a small part of the current flows back to the power supply through L_1 , S1, S2 body diode, and L_2 . The inductor L_1 stores energy during this process.

State II: As shown in Figure 2b, $V_{in} > 0$, the switches S1 and S2 are turned off. During this time, the input current flows through L_1 , D1, the load, and then returns to the power supply through D4. In addition, a small part of the current flows through the body diode of S2 and then flows back to the power supply through L_2 . Later, the inductor L_1 releases energy.

State III: As shown in Figure 2c, $V_{in} < 0$, switch S1 is turned off, and S2 is turned on. During this time, the current flows back to the power supply through L_2 , S2, D3, and a small part of the current flows back to the power supply through L_2 , S2, the body diode of S1 and L_1 , and the inductor L_2 stores energy.

State IV: As shown in Figure 2d, $V_{in} < 0$, the switches S1 and S2 are turned off. During this time, after the input current flows through L_2 , D2, and the load, it flows back to the power supply through D3, and a small part of the current flows back to the power supply through the S1 body diode and L_1 , and the inductor L_2 releases energy.

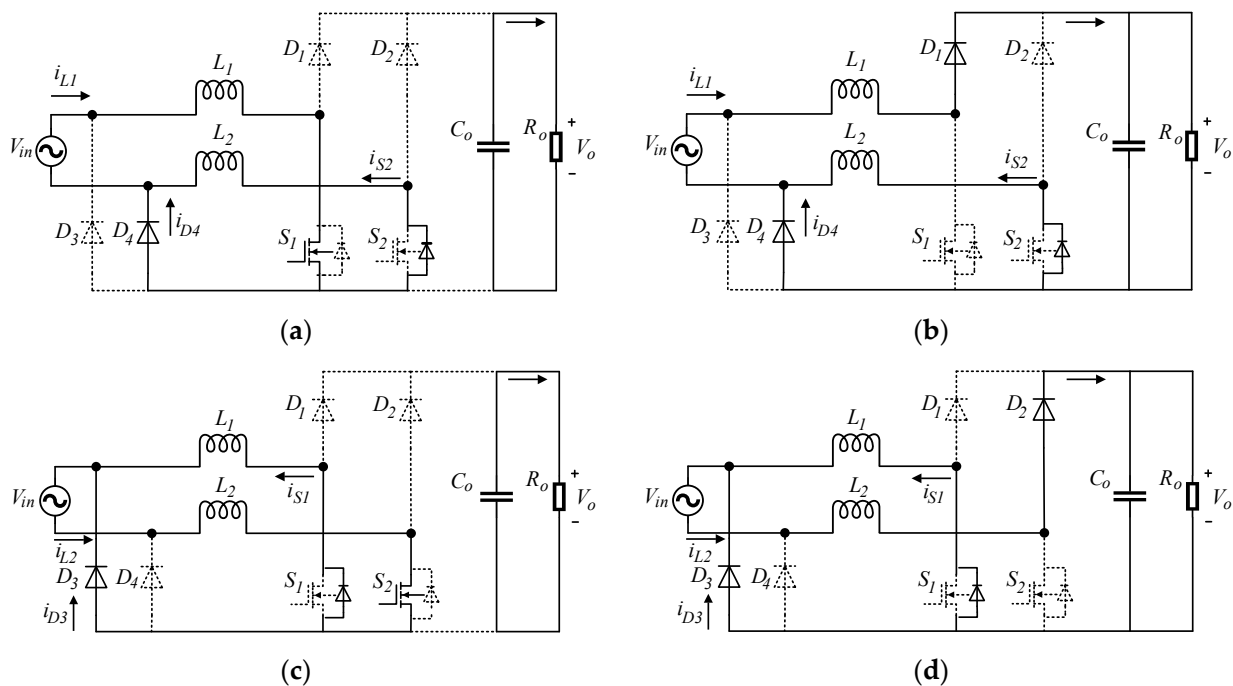


Figure 2. Working state of dual-boost bridgeless PFC converter: (a) $V_{in} > 0$, S1 opens; (b) $V_{in} > 0$, S1 shuts down; (c) $V_{in} < 0$, S2 opens; (d) $V_{in} < 0$, S2 shuts down.

From the above analysis, it can be seen that only two power switches are turned on which is one less than the traditional boost PFC during circuit operation, thus, the on-state loss is smaller, and the efficiency is higher. Also, the common-mode interference of the

circuit is small since the diodes D3 and D4 establish a connection between the input and the output.

2.2. Bridgeless PFC Control Strategy

The dual-boost bridgeless PFC also adopts several commonly used traditional control strategies such as peak current control, average current control, and hysteresis current control which are consistent with the traditional boost PFC. One-cycle control is a nonlinear control strategy, which avoids the use of complex multipliers in traditional control strategies, and has the advantages of fast response, simple circuit implementation, and strong anti-interference ability. During each switching cycle, the one cycle control makes the average value of the switching variable equal or proportional to the control reference value, thereby automatically eliminating the steady-state and transient errors in one cycle, solving the problem of error accumulation in control.

Ideally, the input voltage and current are in the same phase. From the input side, the converter is purely resistive. At this point, the power factor is 1, the circuit satisfies $V_{in} = R_e i_{in}$, V_{in} is the input voltage, R_e is the equivalent resistance of the converter, i_{in} is the PFC input current, and also the inductor current.

For the dual-boost bridgeless PFC converter, the relationship between the input and output voltage and the duty cycle D of the switch is:

$$V_{in} = (1 - D)V_o \quad (1)$$

Define R_s as the resistor used to detect input current of the bridgeless PFC converter. Substitute $V_{in} = R_e i_{in}$ into (1) and multiply both sides by R_s to obtain:

$$R_s i_{in} = \frac{V_o R_s}{R_e} (1 - D) \quad (2)$$

Let $V_m = V_o R_s / R_e$, then:

$$V_m - R_s i_{in} = V_m D \quad (3)$$

where V_m is the modulation voltage.

By (3), we can obtain:

$$V_m - R_s i_{in} = \frac{1}{T} \int_0^{DT} V_m dt \quad (4)$$

where T is one switching cycle.

From (2), it can be known that V_m is the direct voltage, which is proportional to the output voltage V_o . The power factor correction can be realized if the duty cycle D holds (4) to be true. Figure 3 shows its control principle. The PWM controller is composed of a clock and an RS flip-flop. When the rising edge of the clock signal comes, the PWM is at a high level, which turns on the switch. The output signal V_m is obtained after the sampled output voltage passes through the voltage error amplifier, and V_m minus $R_s i_{in}$ forms the left side of (4), and its result is given to the comparator. The inductor stores energy during this time, and the inductor current increases linearly, whereas the difference between the two decreases linearly. The other way passes through the integrator with reset, starting to integrate V_m , its value increases gradually, and finally sends it to the comparator to form the right side of (4). When both sides of the equation are balanced, the output value of the comparator is reversed, which controls the switch to turn off, and the integrator is reset, thereby realizing the control of the duty cycle D .

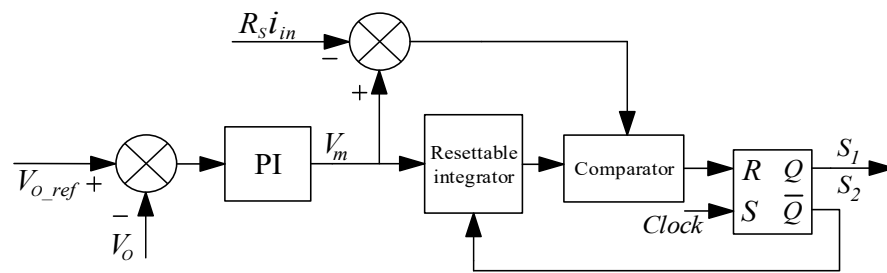


Figure 3. Bridgeless PFC control strategy.

3. Working Principle and Control Strategy of Bidirectional Buck/Boost Power Decoupling Circuit

3.1. Working Principle

In the bridgeless PFC converter, the power factor is assumed to be approximately 1, so the input power on the AC side is:

$$P_{in}(t) = V_{in}(t)i_{in}(t) = \frac{V_{in}I_{in}}{2} - \frac{V_{in}I_{in}}{2} \cos(2\omega t) \quad (5)$$

Then the instantaneous value of DC side output power:

$$P_o(t) = P_{in}(t) + P_o \cos(2\omega t) \quad (6)$$

It can be seen from (6) that the low-frequency ripple on the DC side is generated due to the instantaneous power output containing a double-line-frequency ripple power. Therefore, through the bidirectional buck/boost converter, the ripple power is processed and the low-frequency ripple of the DC output voltage is reduced.

A bidirectional buck/boost converter is a DC/DC converter that can control the bidirectional flow of energy without changing the input and output voltage polarity. The input of the converter is PFC output voltage V_o , and the output is capacitor voltage V_{cs} . It is specified that the transfer of energy from the PFC circuit to the decoupling circuit is positive. As shown in Figure 4, according to the switch state of the switch, the working state of the bidirectional buck/boost converter can be divided into a forwarding switching state, forward continuation state, reverse switching state, and reverse continuation state in a cycle.

Model I: The inductor current is positive, and the converter works in boost mode, while the switch S3 is on. The circuit lies in a forward switching state, and the inductor L_s stores energy.

Model II: The inductor current is positive, the converter works in boost mode, and the switch S3 is turned off. The diode D4 opens and follows the current, the circuit is in a forwarding continuation state, and the PFC converter and inductor L_s supply power to the decoupling capacitor together.

Model III: The inductor current is negative, the converter works in buck mode, and the switch S4 is on. The circuit is in a reverse switching state, the decoupling capacitor simultaneously supplies power to the PFC and the inductor, and the capacitor voltage drops.

Model IV: The inductance current is negative, the converter works in buck mode, and the switch S4 is turned off. The diode D3 opens and follows the current, the circuit is in a reverse continuation state, and the inductance supplies power to the PFC.

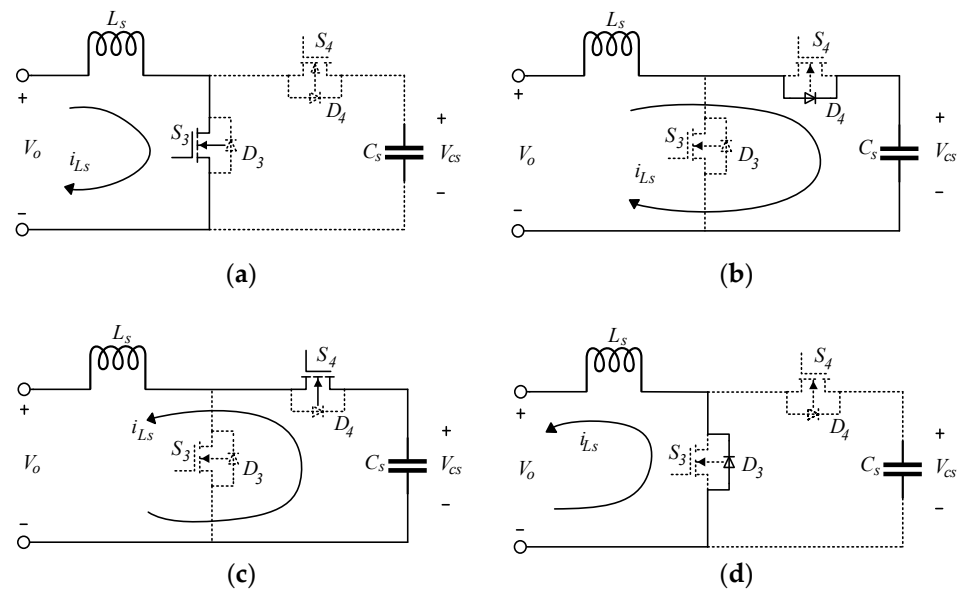


Figure 4. Working mode of the bidirectional buck/boost converter: (a) forward switching state; (b) forward continuation state; (c) reverse switching state; (d) reverse continuation state.

3.2. Control Strategy of Bidirectional Buck/Boost Converter

3.2.1. Bidirectional Buck/Boost Converter Based on Average Current Control

As shown in Figure 5, the double closed-loop control based on average current is a common control in this topology. Since the converter needs to always keep the decoupling capacitor voltage V_{cs} greater than the output voltage V_o of the PFC converter, the voltage outer loop is introduced for control. The output current i_o of the bridgeless PFC converter is collected. Through passive filtering or active filtering, high-pass filtering is performed first, and then low-pass filtering is performed to filter out the high-frequency harmonic component and the DC component in the current, and finally the double-line-frequency current component is obtained. The double-line-frequency current component and the voltage error adjusted by PI (proportional and integral) controller are added as a given current inner loop, and the on/off of the switching tube is controlled so that the power decoupling inductor current follows the double-line-frequency ripple current. Therefore, the bidirectional buck/boost converter produces a double ripple power with the same size and opposite direction as the output end of the bridgeless PFC converter. The output ripple power of the bridgeless PFC converter is offset and the voltage ripple is reduced.

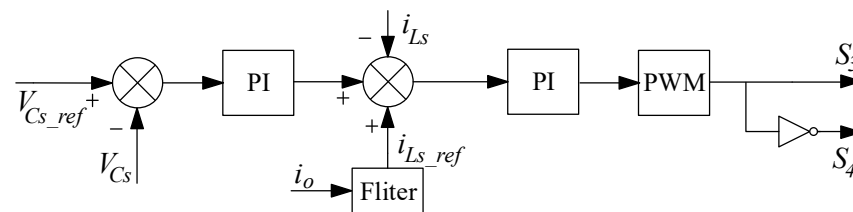


Figure 5. Bidirectional buck/boost converter based on average current control.

3.2.2. Bidirectional Buck/Boost Converter Based on MPCC

In the traditional double closed-loop control, the voltage outer loop and the current inner loop adopt the PI controller. The design process of the parameter of PI controller is complex, the tracking ability of the current inner loop is limited, and the dynamic response speed is poor. To solve this problem, this paper adopts PI control for the voltage outer loop and MPCC for the current inner loop. The control block diagram is shown in Figure 6. The control algorithm includes the establishment of current prediction model and the minimization of cost function. The given current inner loop is the same as the traditional

double closed loop control. Then, according to the input voltage V_o of the bidirectional buck/boost converter obtained by the current cycle sampling, the decoupling inductor current i_{Ls} and the decoupling capacitor voltage V_{cs} , the decoupling inductor current value of the next cycle can be calculated by the prediction model. Finally, a cost function is established to estimate the performance of the converter, and the switching state with the smallest cost function is selected as the control signal of the next sampling period to complete the optimization.

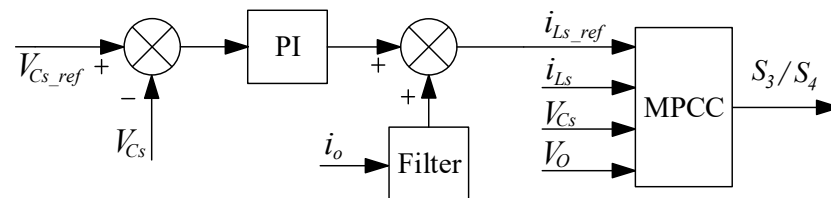


Figure 6. Bidirectional buck/boost converter based on MPCC.

Let the on and off states of the switches S_3 and S_4 be represented by 1 and 0. Figure 4 shows the circuit diagram of the bidirectional buck/boost converter operating in boost mode and buck mode. The current prediction model is established according to its working state.

The equivalent model expression of the bidirectional converter working in boost mode is:

Status I: $S_3 = 1, S_4 = 0$.

The continuous model can be obtained from Figure 4a:

$$L_s \frac{di_{Ls}}{dt} = V_o \tag{7}$$

By discretizing (7) with the forward Euler method, we can obtain:

$$i_{Ls}(k + 1) = \frac{T_s}{L_s} V_o(k) + i_{Ls}(k) \tag{8}$$

where $i_{Ls}(k)$ is the decoupling inductor current value at time k , $i_{Ls}(k + 1)$ is the decoupling inductor current value at time $k + 1$, $V_o(k)$ is the input voltage value at time k , and T_s is the switching period.

Status II: $S_3 = 0, S_4 = 0$.

From Figure 4b, the equivalent circuit expression is:

$$L_s \frac{di_{Ls}}{dt} = V_o - V_{cs} \tag{9}$$

Its discretization model is:

$$i_{Ls}(k + 1) = \frac{T_s}{L_s} (V_o(k) - V_{cs}(k)) + i_{Ls}(k) \tag{10}$$

Similarly, the equivalent model expression of the bidirectional converter operating in buck mode is:

Status III: $S_3 = 0, S_4 = 1$.

From Figure 4c, the equivalent circuit expression is:

$$L_s \frac{di_{Ls}}{dt} = V_{cs} - V_o \tag{11}$$

The discretization of (11) can be obtained:

$$i_{Ls}(k+1) = \frac{T_s}{L_s}(V_{cs}(k) - V_o(k)) + i_{Ls}(k) \quad (12)$$

Status IV: S3 = 0, S4 = 0.

From Figure 4d, the equivalent circuit expression is:

$$L_s \frac{di_{Ls}}{dt} = -V_o \quad (13)$$

The discretization of (13) can be obtained:

$$i_{Ls}(k+1) = -\frac{T_s}{L_s}V_o(k) + i_{Ls}(k) \quad (14)$$

Equations (8), (10), (12) and (14) are the prediction models of bidirectional buck/boost converter. Combining the above equations, and assuming that the duty cycle of the switch S3 is d_3 and the duty cycle of the switch S4 is d_4 , the average discrete model of the bidirectional buck/boost converter in boost mode and buck mode can be obtained:

$$i_{Ls_Boost}(k+1) = \frac{T_s}{L_s}(V_o(k) + (d_3 - 1)V_{cs}(k)) + i_{Ls}(k) \quad (15)$$

$$i_{Ls_Buck}(k+1) = \frac{T_s}{L_s}(d_4V_{cs}(k) - V_o(k)) + i_{Ls}(k) \quad (16)$$

In order to select the best working state, the cost function in boost and buck modes is defined as:

$$J_{Boost} = (i_{Ls_Boost}(k+1) - i_{Ls_ref})^2 \quad (17)$$

$$J_{Buck} = (i_{Ls_Buck}(k+1) - i_{Ls_ref})^2 \quad (18)$$

Substitute (15) and (16) into (17) and (18) to obtain:

$$J_{Boost} = \left(\frac{T_s}{L_s}(V_o(k) + (d_3 - 1)V_{cs}(k)) + i_{Ls}(k) - i_{Ls_ref}\right)^2 \quad (19)$$

$$J_{Buck} = \left(\frac{T_s}{L_s}(d_4V_{cs}(k) - V_o(k)) + i_{Ls}(k) - i_{Ls_ref}\right)^2 \quad (20)$$

As shown in Figure 7, it is the control flow chart of the bidirectional buck/boost converter based on the model predictive current control. Firstly, according to the input parameter $V_o(k)$, the values of $V_o(k)$ and V_{o_ave} are compared, where V_{o_ave} is the average value of the output voltage of the PFC converter, and the value is 400 V. When $V_o(k) > V_{o_ave}$, the bidirectional converter works in boost mode, capacitor stores energy; when $V_o(k) < V_{o_ave}$, the bidirectional converter works in buck mode, and the capacitor releases energy. Then, according to the respective prediction models and cost functions of the two modes, the action of the switch is controlled. For example, when the bidirectional converter works in boost mode, according to (19), the corresponding values of $J_{boost_s3=0}$ and $J_{boost_s3=1}$ are calculated, respectively, for comparison, and the on/off state of switch corresponding to the smaller value is taken as the action state of S3 at the next time, and then the on/off of S3 is controlled, so that the decoupling capacitor absorbs the double-line-frequency ripple power. The same occurs for the bidirectional converter operating in buck mode.

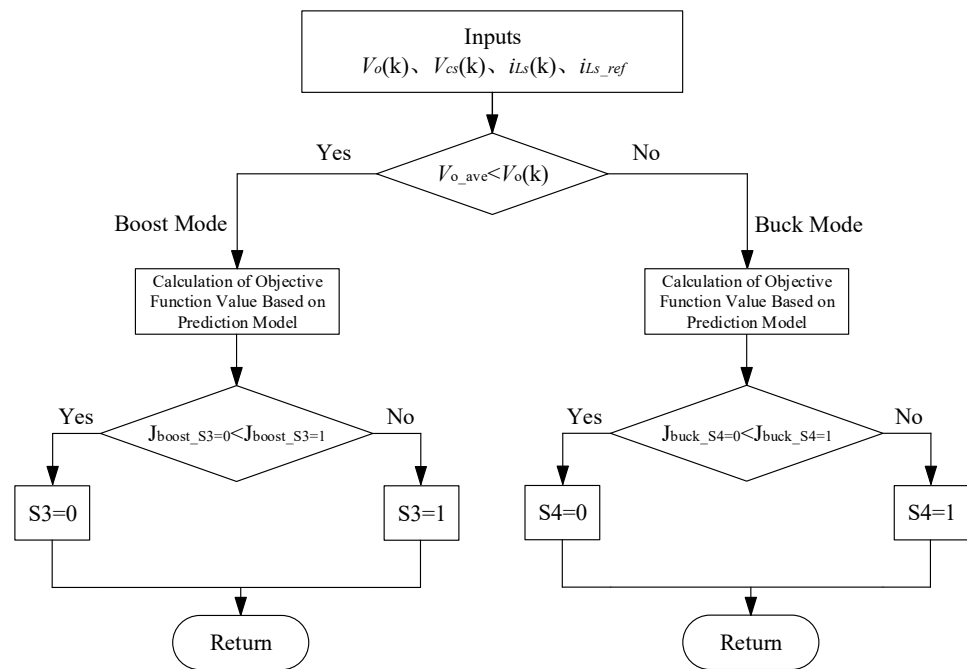


Figure 7. Flow chart of model predictive current control.

3.3. Main Parameter Design

It can be seen from Figure 8 that V_{cs_ave} is the average value of the decoupling capacitor voltage, V_{cs_max} is the maximum capacitor voltage, and V_{cs_min} is the minimum capacitor voltage, where $\Delta V_{cs} = V_{cs_max} - V_{cs_min}$. In the period of $[T/8 \ 3T/8]$, $P_{in} > P_o$, capacitance C_s is charged. In the period of $[3T/8 \ 5T/8]$, $P_{in} < P_o$, capacitance C_s is discharged. The energy absorbed by the decoupling capacitor in $[T/8 \ 3T/8]$ can be calculated as follows:

$$\Delta E = \int_{T/8}^t [P_{in}(t) - P_o(t)]dt = - \int_{T/8}^t P_o \cos 2\omega t dt = \frac{P_o}{\omega} \sin^2(\omega t - \frac{\pi}{4}) \quad (21)$$

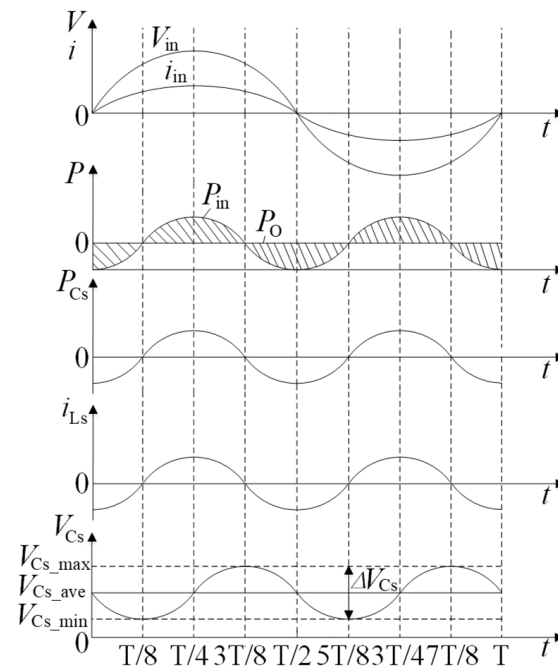


Figure 8. Waveforms of V_{in} , i_{in} , P_{in} , P_o , V_{cs} .

Another expression of ΔE is:

$$\Delta E = \frac{1}{2}C_s(V_{cs}^2(t) - V_{cs_min}^2) \tag{22}$$

(21) and (22) can be combined to:

$$V_{cs}(t) = \sqrt{\frac{2P_o \sin^2(\omega t - \frac{\pi}{4})}{\omega C_s} + V_{cs_min}^2} \tag{23}$$

Substituting $t = 3T/8$ into (21) yields:

$$\Delta E = \int_{T/8}^{3T/8} (P_{in}(t) - P_o(t))dt = - \int_{T/8}^t P_o \cos^2 \omega t dt = \frac{P_o}{\omega} \sin^2(\omega t - \frac{\pi}{4}) \tag{24}$$

The ΔE is:

$$\Delta E = \frac{1}{2}C_s(V_{cs_max}^2 - V_{cs_min}^2) \tag{25}$$

(24) and (25) can be combined to:

$$C_s = \frac{2P_o}{\omega(V_{cs_max}^2 - V_{cs_min}^2)} = \frac{P_o}{\omega \Delta V_{cs} (\frac{V_{cs_max} + V_{cs_min}}{2})} \tag{26}$$

Considering the voltage V_{Cs_min} in (26) as 440 V, we can obtain:

$$V_{cs_max} = \sqrt{\frac{2P_o}{\omega C_s} + V_{cs_min}^2} \tag{27}$$

The decoupling capacitor voltage is:

$$V_{cs} = \frac{V_{cs_max} + V_{cs_min}}{2} = \frac{V_{cs_min} + \sqrt{\frac{2P_o}{\omega C_s} + V_{cs_min}^2}}{2} \tag{28}$$

Substituting $P_o = 210$ W, $V_{Cs_min} = 440$ V into (27) and (28), we can obtain Figure 9. It can be seen from the figure that when the capacitance value is small, the voltage fluctuates greatly. When the capacitance increases, the voltage fluctuation range gradually decreases. Considering the relationship between capacitance and the voltage stress, the decoupling capacitor $C_s = 15\mu\text{F}$ is selected. Substituting the capacitance value into equations (27) and (28), we can find the maximum decoupling capacitor voltage $V_{Cs_max} = 530$ V, $V_{Cs} = 485$ V.

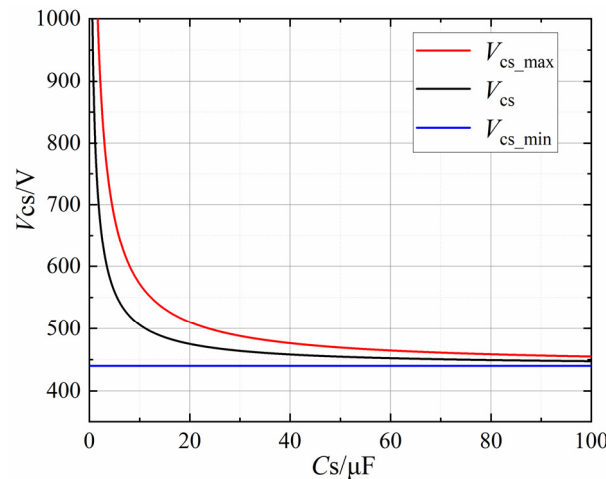


Figure 9. The relationship between voltage and capacitance of the decoupling capacitor.

Switch S3, S4 complementary conduction, according to the relationship between input voltage and output voltage of the bidirectional converter, the duty cycle of S3 can be expressed as:

$$d_3 = 1 - \frac{V_o}{V_{cs}(t)} \quad (29)$$

When S3 is turned on, the amount of change in i_{Ls} is:

$$\Delta i_{Ls} = \frac{V_o}{L_s} d_3 T \quad (30)$$

Combining (29) and (30), from the inductance current is not greater than the maximum ripple current Δi_{Ls_max} , we can obtain:

$$L_s \geq \frac{(V_{cs}(t) - V_o) V_o T}{V_{cs}(t) \Delta i_{Ls_max}} \quad (31)$$

The decoupling inductance selected in this paper is 2 mH.

4. Simulation and Experimental Analysis

First, the simulation model of the dual-boost bridgeless PFC converter based on one cycle control is established in Matlab/Simulink, and the influence of capacitance on the PFC circuit is analyzed by changing the capacitance of the output filter. On this basis, the power decoupling circuit is added, and its simulation model and experimental platform based on MPCC is built to verify the effectiveness and superiority of the theory. Table 1 shows the main simulation parameters in this paper.

Table 1. Main simulation parameters.

Main Parameters	Value
RMS Input voltage, V_{in}	220 V/50 Hz
Output voltage, V_o	400 V
Power, P_o	210 W
Inductance, L_1, L_2	1.25 mH
Inductance L_s	2 mH
Capacitance without power decoupling circuit C_o	220 μ F
Capacitance after adding power decoupling circuit C_o	40 μ F
Capacitance C_s	15 μ F
Switching frequency of bridgeless PFC converter	100 KHz
Switching frequency of power decoupling circuit	50 KHz

4.1. Simulation of One Cycle Control Bridgeless PFC Converter

The input voltage, current, and output voltage waveforms of bridgeless PFC converters without a power decoupling circuit are shown in Figure 10. The input voltage reduced by a factor of 100 for ease of observation and the circuit can satisfactorily realize power factor correction while using one cycle control. During this time, the filter capacitor $C_o = 220 \mu$ F, the output voltage is stable at 400 V and fluctuates around ± 5 V, and the voltage ripple coefficient $\gamma = 1.25\%$.

From Figure 11, it can be seen that when the value of capacitance is changed, when the capacitance $C_o = 220 \mu$ F, the output voltage fluctuation is ± 5 V and the voltage ripple coefficient is $\gamma = 1.25\%$. The ripple coefficient does not meet the circuit requirements when the capacitance $C_o = 40 \mu$ F, the output voltage fluctuation reaches ± 27 V and the voltage ripple coefficient $\gamma = 6.75\%$. From the current manufacturing process, most of the ones above 100 μ F are electrolytic capacitors, while the traditional PFC often realizes power factor correction by connecting the electrolytic capacitor at the output end. To realize no electrolytic capacitor and improve the service life of converter, it is necessary to adopt an appropriate power decoupling circuit and control method.

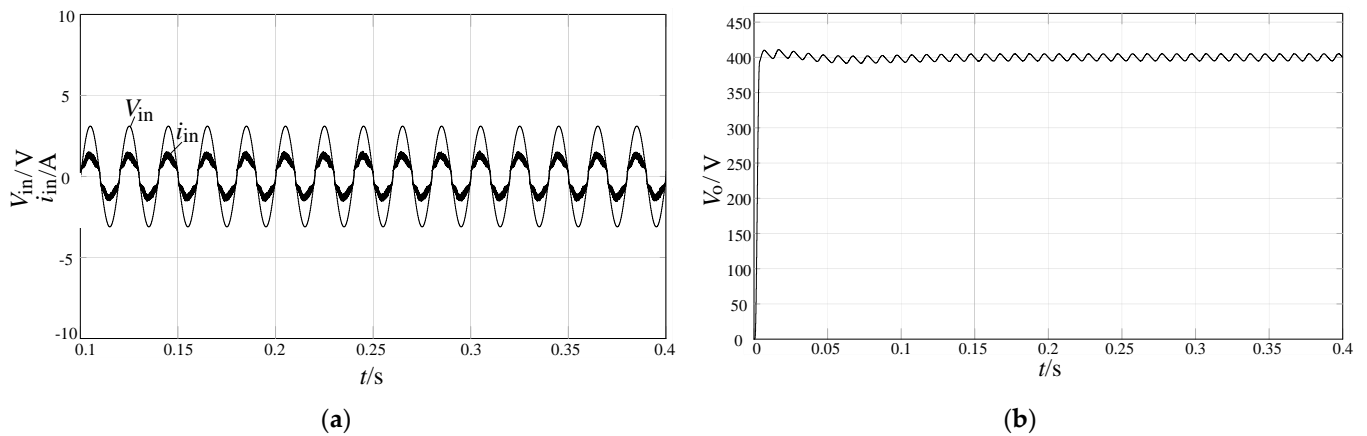


Figure 10. Input voltage, current, and output voltage waveforms of bridgeless PFC converter without power decoupling circuit: (a) input voltage and input current; (b) output voltage.

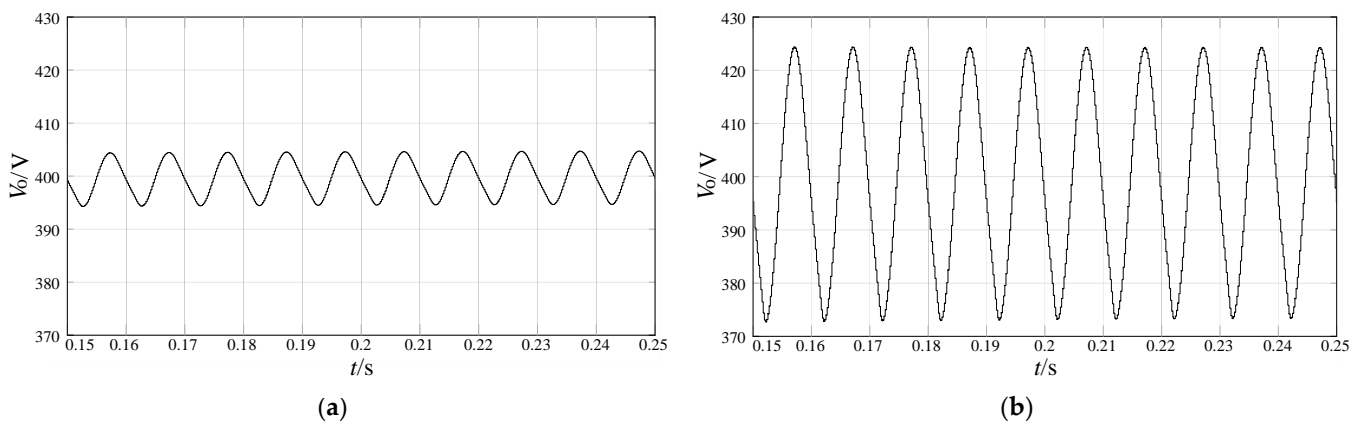


Figure 11. Output voltage ripple of bridgeless PFC converter under different capacitance values: (a) output filter capacitance $C_o = 220 \mu\text{F}$; (b) output filter capacitance $C_o = 40 \mu\text{F}$.

4.2. Simulation of Power Decoupling Circuit for Model Predictive Current Control

Figure 12 shows the input voltage and current waveform of a bridgeless PFC converter after adding the bidirectional buck/boost converter. The effective value of the input voltage is 220 V, which is scaled down to 1:100. It can be seen that the input current follows the input voltage, the power factor up to 0.999, which can well achieve power factor correction. The addition of the bidirectional buck/boost converter does not affect the power factor correction of the bridgeless PFC converter.

Figure 13 shows a comparison of the output voltage waveforms without the power decoupling circuit and with the power decoupling circuit when the output filter capacitor $C_o = 40 \mu\text{F}$. It can be seen that when the power decoupling circuit is not added, the fluctuation range of the output voltage reaches $\pm 27 \text{ V}$ and the voltage ripple coefficient $\gamma = 6.75\%$, which cannot meet the circuit requirements. After adding the power decoupling circuit, the ripple of the output voltage is obviously reduced, and the voltage fluctuates around $\pm 2.5 \text{ V}$ with a voltage ripple coefficient of $\gamma = 0.625\%$, and comparing with Figure 8b, it can be seen that the power decoupling solution can be equated to the solution with a large $220 \mu\text{F}$ traditional electrolytic capacitor, and its ripple is lower than the traditional solution.

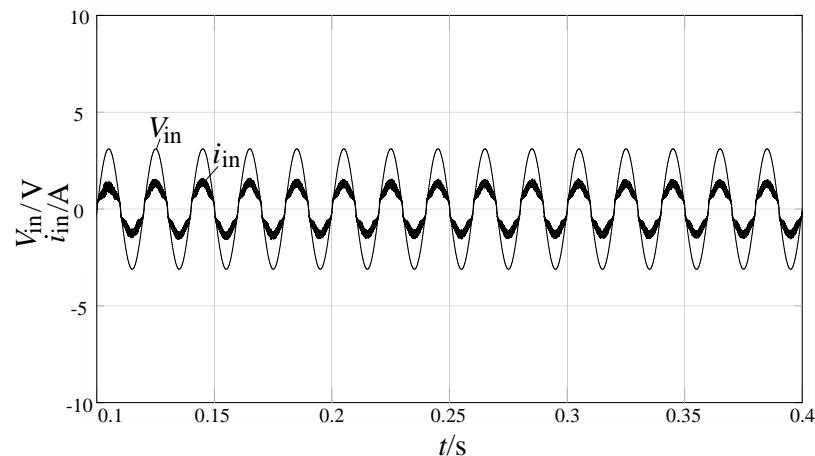


Figure 12. Input voltage and current waveforms of the bridgeless PFC converter with bidirectional buck/boost converter.

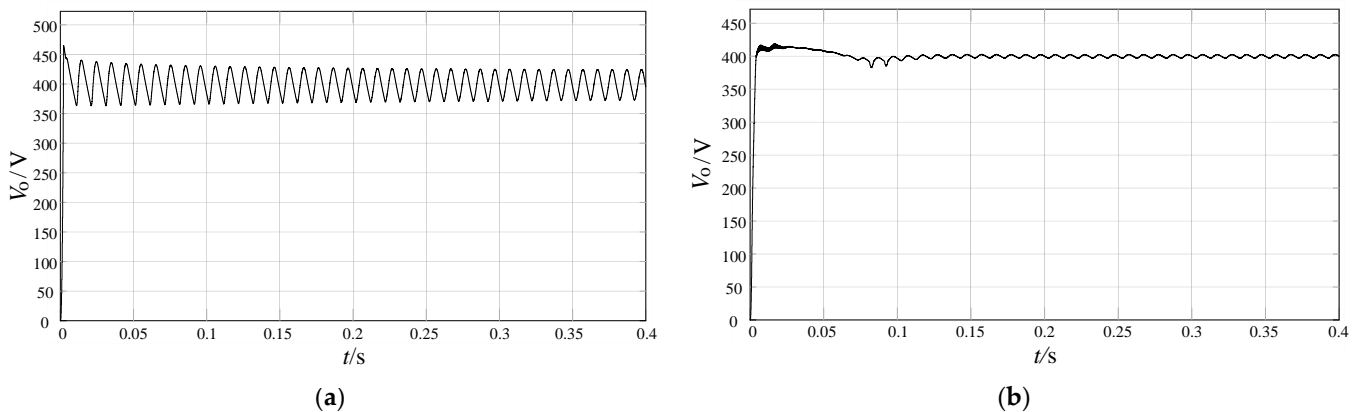


Figure 13. Output voltage waveforms of the bridgeless PFC converter: (a) bidirectional buck/boost converter is not contained; (b) bidirectional buck/boost converter is contained.

As shown in Figure 14a, the output voltage ripple waveform after adding the bidirectional buck/boost converter, it can be seen that the voltage fluctuates around ± 2.5 V; comparing with Figure 11b, it can be found that the output voltage fluctuation is significantly reduced. In the meanwhile, the capacitors used in the system are film capacitors, so it can well achieve being electrolytic capacitor-less. Figure 14b shows the voltage waveform of the power decoupling capacitor. It can be seen that the voltage of the decoupling capacitor fluctuates around ± 45 V, with an average voltage of around 485 V. At this time, the voltage fluctuation range is large, so the decoupling capacitor uses the thin film capacitor with small capacitance value.

As shown in Figure 15a,b, the output voltage fluctuates when the load changes. It can be seen from the figure that when the load changes from full load to half load and load changes from half load to full load, the output voltage can be restored to a stable state within 0.02 s, and the voltage does not fluctuate significantly when the load changes. Figure 15c,d are the waveforms of the output current when the load changes abruptly. The current can reach stability quickly after the load changes, so the dynamic response speed of the system is fast and the dynamic stability is strong.

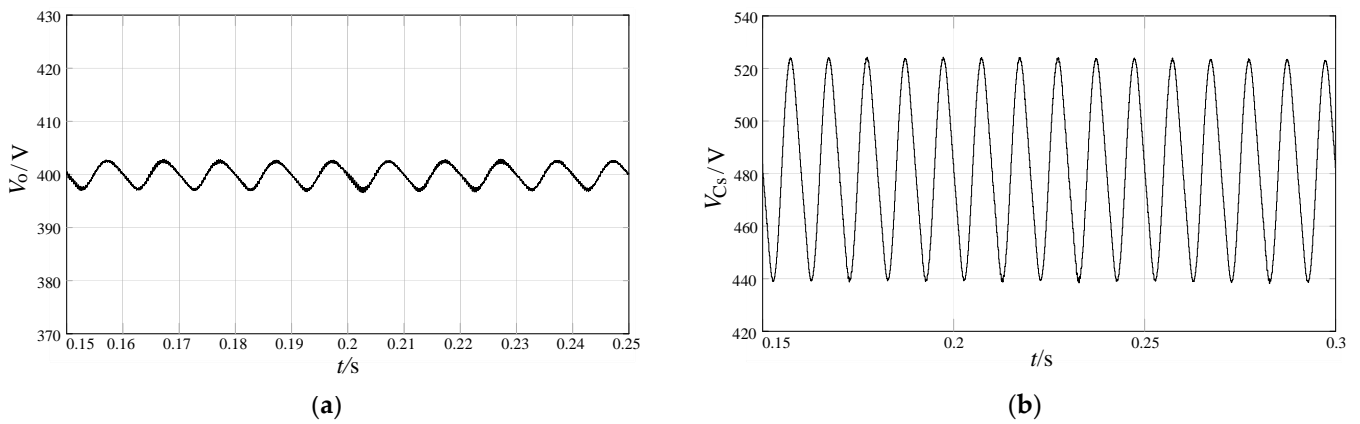


Figure 14. The output voltage waveforms of the bridgeless PFC converter and power decoupling circuit: (a) output voltage ripple; (b) power decoupling capacitor voltage.

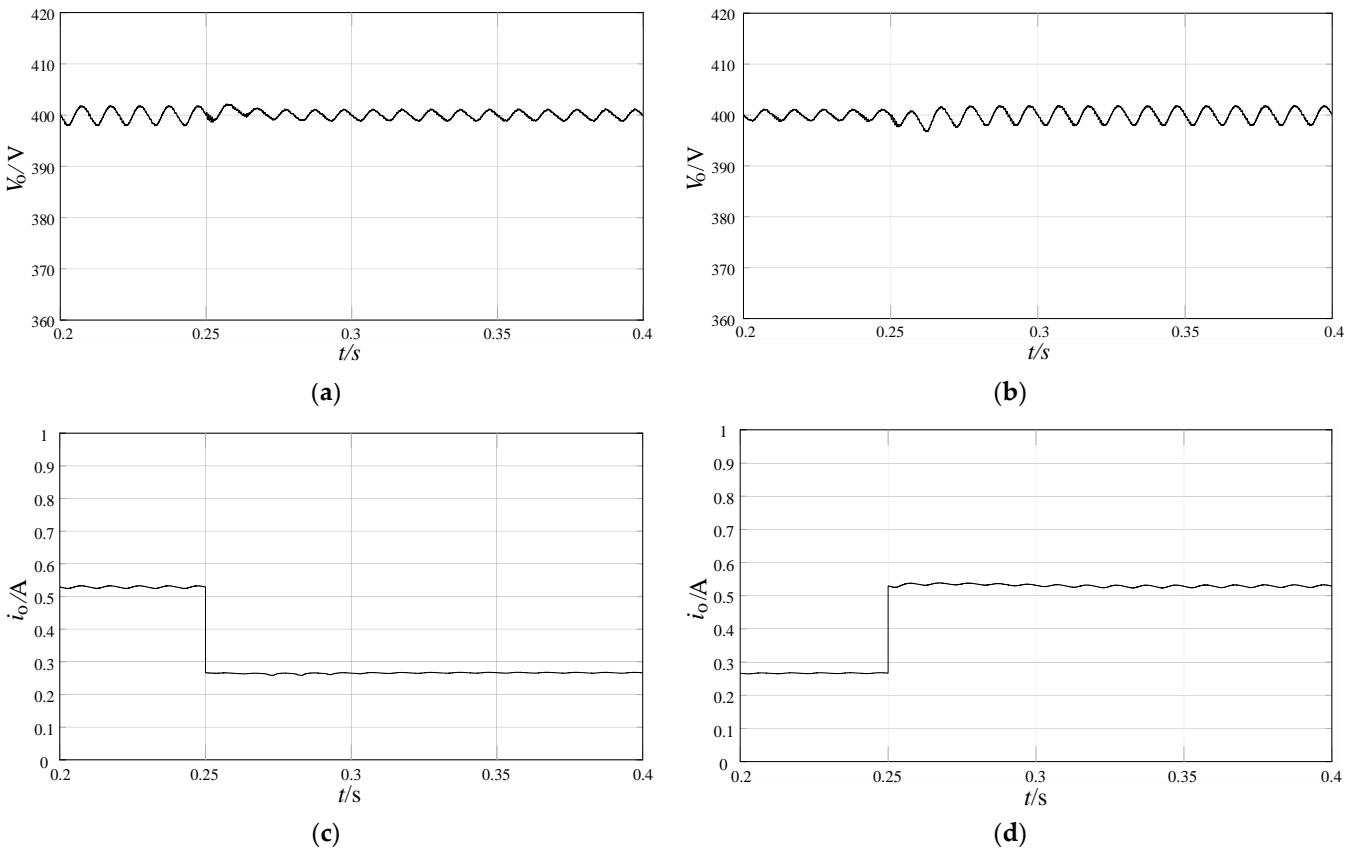


Figure 15. Output voltage and current waveforms when the load is abrupt: (a) voltage waveform at full load burst to half load; (b) voltage waveform at half load burst to full load; (c) current waveform at full load burst to half load; (d) current waveform at half load burst to full load.

Figure 16 shows the inductor current waveforms of the power decoupling circuit when different control strategies are used. As shown in Figure 16a, the conventional double closed-loop control is used, which has limited tracking capability in the inner loop of the current, and in Figure 16b, the inner loop of the current is controlled by model current prediction control, which, as can be seen from the figure, has a better current tracking effect and can make the bidirectional buck/boost converter absorb two times the ripple component of the power frequency and reduce the ripple at the output.

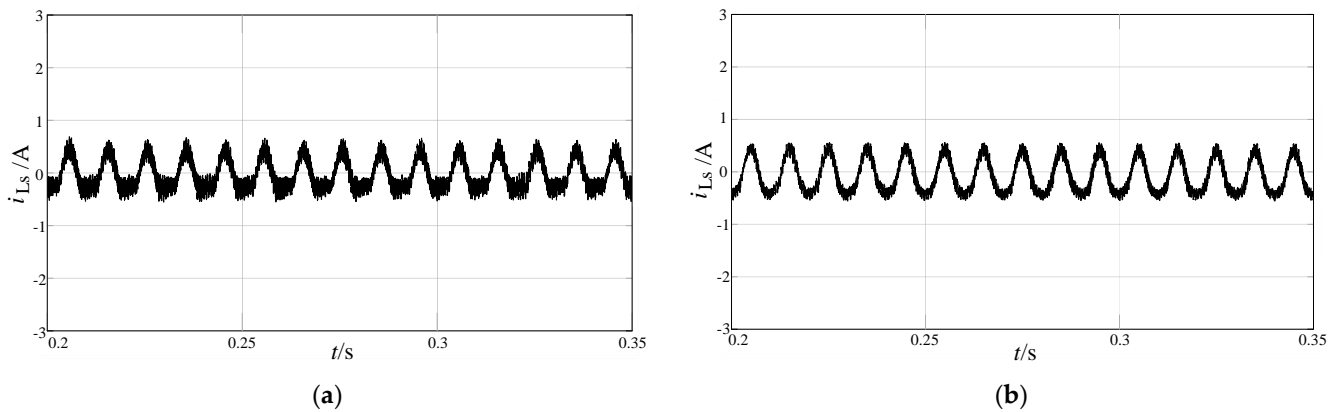


Figure 16. Power decoupling circuit inductor current: (a) conventional double closed-loop control; (b) model current prediction control.

Figure 17 shows the output current ripple. Figure 17a shows the current ripple when using the traditional double closed-loop control, the current pulsation Δi_o is 0.03 A, which is about 5.7% of the average current value of 0.525 A, while the output current pulsation Δi_o of the current inner loop proposed in this paper is 0.008 A using the model predictive current control, which is about 1.5% of the average current value of 0.525 A. This comparison shows that the output current ripple is smaller with the model predictive current control.

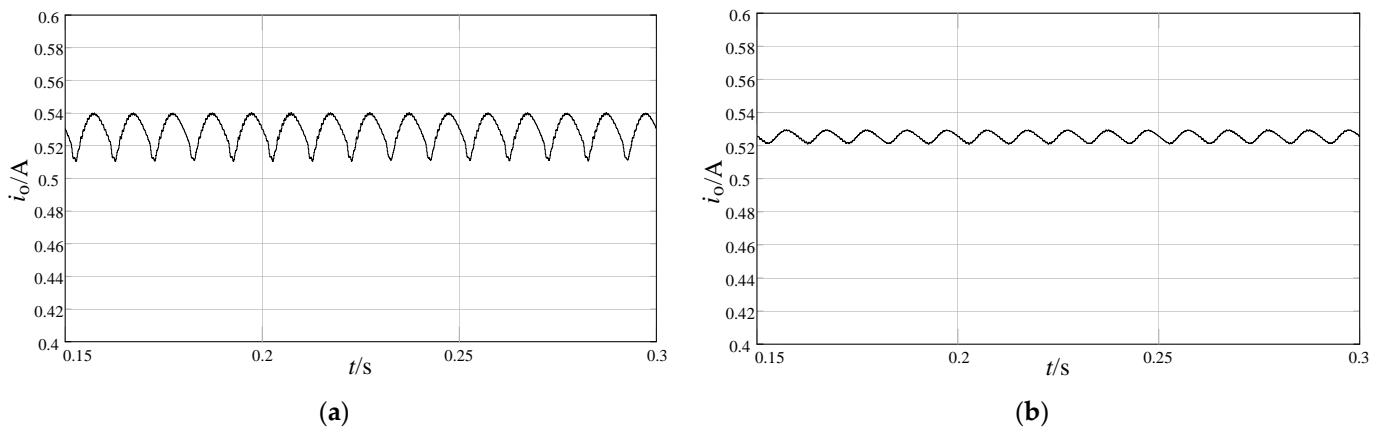


Figure 17. Output current ripple: (a) conventional double closed-loop control; (b) model current prediction control.

4.3. Experimental Analysis

The input voltage and current waveforms of the bridgeless PFC converter are shown in Figure 18. The input voltage and current peaks in the figure are about 311 V and 1.4 A, and the effective values are about 220 V and 1 A, so the input power is about 220 W. The current changes in the form of sine wave following the voltage phase.

The input current waveform of the bidirectional buck/boost converter is shown in Figure 19. It can be seen that the amplitude of the decoupling inductor current i_{Ls} is about 0.5 A, and the frequency is double-line-frequency, that is, 100 Hz. Therefore, the bidirectional buck/boost converter can effectively absorb double-line-frequency ripple.

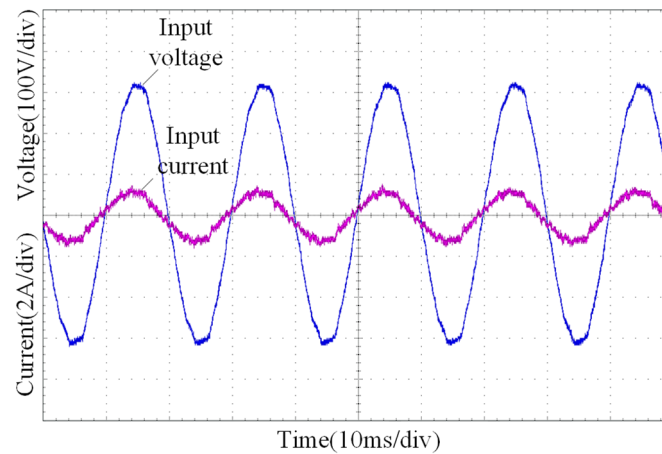


Figure 18. Input voltage and current waveform of bridgeless PFC with power decoupling circuit.

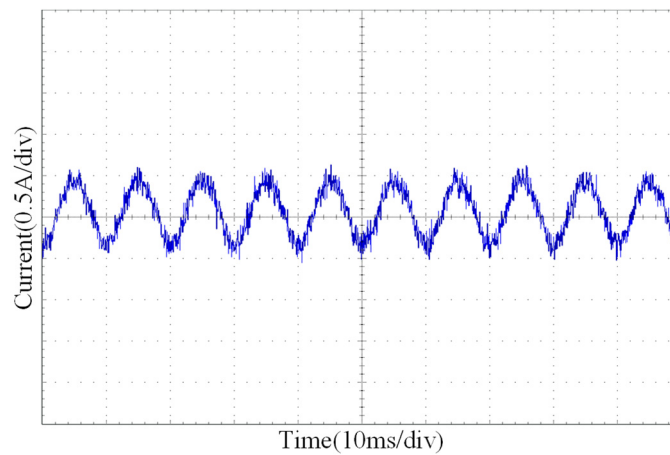


Figure 19. Decoupling inductor current waveform.

As shown in Figure 20, the output voltage ripple of the bridgeless PFC converter can be obtained. The output voltage fluctuates around ± 4 V, and the voltage ripple coefficient $\gamma = 1\%$, which meets the design requirements of this paper. At this time, the capacitors in the circuit use small-capacitance film capacitors to achieve no electrolytic capacitors.

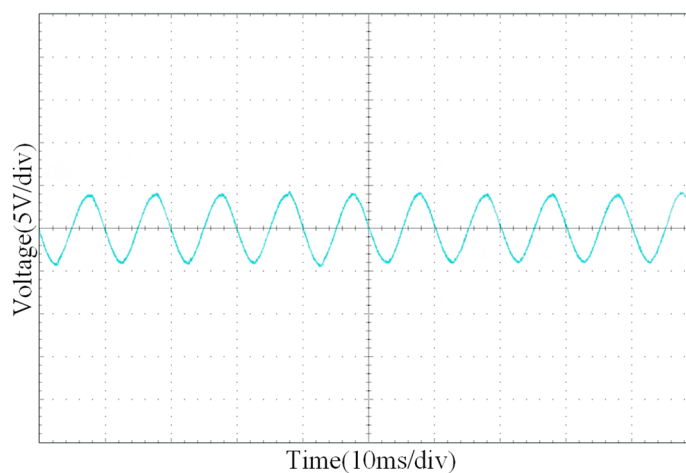


Figure 20. Output voltage ripple waveform of bridgeless PFC.

5. Conclusions

In this paper, the dual-boost bridgeless PFC converter based on one cycle control with a power decoupling circuit was used for suppressing the ripple of the output power. The power decoupling circuit adopted PI control for the voltage outer loop and MPCC for the current inner loop, which essentially improved the utilization of the capacitor and realized non-electrolytic capacitor. Finally, the effectiveness of the theoretical analysis was verified via simulations and experiments. In this paper, two film capacitors were used for replacement of the traditional large electrolytic capacitor, which greatly improved the service life of the converter, and well realized power factor correction and the non-electrolytic capacitance of the PFC converter, which has very important practical value.

Author Contributions: Conceptualization, N.-Z.J. and Z.-Q.W.; methodology, N.-Z.J. and Z.-Q.W.; software, Z.-Q.W., L.Z. and Y.F.; validation, Z.-Q.W., L.Z. and Y.F.; supervision, N.-Z.J. and X.-G.W.; writing—original draft, Z.-Q.W.; writing—review and editing, N.-Z.J., Z.-Q.W. and X.-G.W. All authors have read and agreed to the published version of the manuscript.

Funding: This research was funded by the Open Fund Project of State Key Laboratory of Automotive Safety and Energy, grant number KFY2222.

Conflicts of Interest: The authors declare no conflict of interest. The funders had no role in the design of the study; in the collection, analysis, or interpretation of data; in the writing of the manuscript, or in the decision to publish the results.

References

1. Sharma, G.; Sood, V.K.; Alam, M.S.; Shariff, S.M. Comparison of common DC and AC bus architectures for EV fast charging stations and impact on power quality. *eTransportation* **2020**, *5*, 100066. [[CrossRef](#)]
2. Guo, C.L.; Zhu, K.J.; Chen, C.C.; Xiao, X.N. Characteristics and effect laws of the large-scale electric Vehicle's charging load. *eTransportation* **2020**, *3*, 100049. [[CrossRef](#)]
3. Zhao, B.; Abramovitz, A.; Smedley, K. Family of Bridgeless Buck-Boost PFC Rectifiers. *IEEE Trans. Power Electron.* **2015**, *30*, 6524–6527. [[CrossRef](#)]
4. Fardoun, A.A.; Ismail, E.H.; Sabzali, A.J.; Al-Saffar, M.A. New Efficient Bridgeless Cuk Rectifiers for PFC Applications. *IEEE Trans. Power Electron.* **2012**, *27*, 3292–3301. [[CrossRef](#)]
5. Kim, Y.S.; Sung, W.Y.; Lee, B.K. Comparative Performance Analysis of High Density and Efficiency PFC Topologies. *IEEE Trans. Power Electron.* **2014**, *29*, 2666–2679. [[CrossRef](#)]
6. Singh, B.; Kushwaha, R. A PFC Based EV Battery Charger Using a Bridgeless Isolated SEPIC Converter. *IEEE Trans. Ind. Appl.* **2020**, *56*, 477–487. [[CrossRef](#)]
7. Bang, T.; Park, J.W. Development of a ZVT-PWM Buck Cascaded Buck-Boost PFC Converter of 2 Kw with the Widest Range of Input Voltage. *IEEE Trans. Ind. Electron.* **2018**, *65*, 2090–2099. [[CrossRef](#)]
8. Yu, Z.W.; Xia, Y.L.; Ayyanar, R. A Simple ZVT Auxiliary Circuit for Totem-Pole Bridgeless PFC Rectifier. *IEEE Trans. Ind. Appl.* **2019**, *55*, 2868–2878. [[CrossRef](#)]
9. Hawkins, N.S.; McIntyre, M.L.; Latham, J.A. Nonlinear Control for Power Factor Correction of a Dual-Boost Bridgeless Circuit. In Proceedings of the IECON 2018—44th Annual Conference of the IEEE Industrial Electronics Society, Washington, DC, USA, 21–23 October 2018; pp. 1368–1373.
10. Huber, L.; Jang, Y.; Jovanovic, M.M. Performance Evaluation of Bridgeless PFC Boost Rectifiers. *IEEE Trans. Power Electron.* **2008**, *23*, 1381–1390. [[CrossRef](#)]
11. Mahdavi, M.; Farzanehfard, H. Bridgeless SEPIC PFC Rectifier with Reduced Components and Conduction Losses. *IEEE Trans. Ind. Electron.* **2011**, *58*, 4153–4160. [[CrossRef](#)]
12. Pastor, A.M.; Idiarte, E.V.; Pastor, A.C.; Salamero, L.M. Loss-Free Resistor-Based Power Factor Correction Using a Semi-Bridgeless Boost Rectifier in Sliding-Mode Control. *IEEE Trans. Power Electron.* **2015**, *30*, 5842–5853. [[CrossRef](#)]
13. Alam, M.; Eberle, W.; Gautam, D.S.; Botting, C. A Soft-Switching Bridgeless AC–DC Power Factor Correction Converter. *IEEE Trans. Power Electron.* **2016**, *32*, 7716–7726. [[CrossRef](#)]
14. Xu, X.L.; Liu, J.; Zhang, Y.G. Research of current hysteresis control for boost bridgeless PFC. In Proceedings of the 2018 13th IEEE Conference on Industrial Electronics and Applications (ICIEA), Wuhan, China, 31 May–2 June 2018; pp. 265–269.
15. Etz, R.; Patarau, T.; Petreus, D. Comparison between digital average current mode control and digital one cycle control for a bridgeless PFC boost converter. In Proceedings of the 2012 IEEE 18th International Symposium for Design and Technology in Electronic Packaging (SIITME), Alba Iulia, Romania, 25–28 October 2012; pp. 211–215.
16. Wang, A.; Huang, F.Y.G.; Zhao, B. A Bridgeless Cuk PFC Converter Based on One Cycle Control. In Proceedings of the 2020 Chinese Automation Congress (CAC), Shanghai, China, 6–8 November 2020; pp. 4674–4678.

17. Deng, K.; Peng, H.J.; Dirkes, S.; Gottschalk, J.; Unlubayir, C.; Thul, A.; Lowenstein, L.; Pischinger, S.; Hameyer, K. An adaptive PMP-based model predictive energy management strategy for fuel cell hybrid railway vehicles. *eTransportation* **2021**, *7*, 100094. [[CrossRef](#)]
18. Liu, J.Z.; Wang, Z.P.; Hou, Y.K.; Qu, C.H.; Hong, J.C.; Lin, N. Data-driven energy management and velocity prediction for four-wheel-independent-driving electric vehicles. *eTransportation* **2021**, *9*, 100119. [[CrossRef](#)]
19. Cecati, C.; Ciancetta, F.; Siano, P. A Multilevel Inverter for Photovoltaic Systems with Fuzzy Logic Control. *IEEE Trans. Ind. Electron.* **2010**, *57*, 4115–4125. [[CrossRef](#)]
20. Cao, L.L.; Zhu, Y.C.; Wu, H. A New Electrolytic Capacitor-less LED Driver with Coupled-Inductor. In Proceedings of the 2020 IEEE Applied Power Electronics Conference and Exposition (APEC), New Orleans, LA, USA, 15–19 March 2020; pp. 1537–1543.
21. Luo, Q.M.; Huang, J.; He, Q.Q.; Ma, K.; Zhou, L.W. Analysis and Design of a Single-Stage Isolated AC–DC LED Driver with a Voltage Doubler Rectifier. *IEEE Trans. Ind. Electron.* **2017**, *64*, 5807–5817. [[CrossRef](#)]
22. Fukushima, K.; Norigoe, I.; Shoyama, M.; Ninomiya, T.; Harada, Y.; Tsukakoshi, K. Input Current-Ripple Consideration for the Pulse-link DC-AC Converter for Fuel Cells by Small Series LC Circuit. In Proceedings of the 2009 Twenty-Fourth Annual IEEE Applied Power Electronics Conference and Exposition, Washington, DC, USA, 15–19 February 2009; pp. 447–451.
23. Gu, L.L.; Ruan, X.B.; Xu, M.; Yao, K. Means of Eliminating Electrolytic Capacitor in AC/DC Power Supplies for LED Lightings. *IEEE Trans. Power Electron.* **2009**, *24*, 1399–1408. [[CrossRef](#)]
24. Tang, Y.; Blaabjerg, F.; Loh, P.C.; Jin, C.; Wang, P. Decoupling of Fluctuating Power in Single-Phase Systems Through a Symmetrical Half-Bridge Circuit. *IEEE Trans. Power Electron.* **2015**, *30*, 1855–1865. [[CrossRef](#)]
25. Liu, Y.L.; Sun, Y.; Su, M.; Zhou, M.; Zhu, Q.; Li, X. A Single-Phase PFC Rectifier with Wide Output Voltage and Low-Frequency Ripple Power Decoupling. *IEEE Trans. Power Electron.* **2018**, *33*, 5076–5086. [[CrossRef](#)]
26. Su, M.; Pan, P.; Long, X.; Sun, Y.; Yang, J. An Active Power-Decoupling Method for Single-Phase AC–DC Converters. *IEEE Trans. Ind. Inform.* **2014**, *10*, 461–468. [[CrossRef](#)]
27. Li, H.B.; Zhang, K.; Zhao, H.; Fan, S.F.; Xiong, J. Active Power Decoupling for High-Power Single-Phase PWM Rectifiers. *IEEE Trans. Power Electron.* **2013**, *28*, 1308–1319. [[CrossRef](#)]
28. Harb, S.; Balog, R.S. Single-phase PWM rectifier with power decoupling ripple-port for double-line-frequency ripple cancellation. In Proceedings of the 2013 Twenty-Eighth Annual IEEE Applied Power Electronics Conference and Exposition, Long Beach, CA, USA, 17–21 March 2013; pp. 1025–1029.
29. Wang, R.X.; Wang, F.; Boroyevich, D.; Burgos, R.; Lai, R.X.; Ning, P.Q.; Rajashekara, K. A High Power Density Single-Phase PWM Rectifier with Active Ripple Energy Storage. *IEEE Trans. Power Electron.* **2011**, *26*, 1430–1443. [[CrossRef](#)]
30. Cao, X.; Zhong, Q.C.; Ming, W.L. Ripple Eliminator to Smooth DC-Bus Voltage and Reduce the Total Capacitance Required. *IEEE Trans. Ind. Electron.* **2015**, *62*, 2224–2235. [[CrossRef](#)]

Disclaimer/Publisher’s Note: The statements, opinions and data contained in all publications are solely those of the individual author(s) and contributor(s) and not of MDPI and/or the editor(s). MDPI and/or the editor(s) disclaim responsibility for any injury to people or property resulting from any ideas, methods, instructions or products referred to in the content.